Desalination and Water Treatment
www.deswater.com

doi:10.5004/dwt.2018.22486

120 (2018) 73–87
July

High water flux poly(acrylonitrile-co-methyl acrylate) membranes fabricated via thermally induced phase separation

Linli Tan, Na Han*, Longfei Zhang, Zhenyu Cui, Wei Li, Xingxiang Zhang*, Jun Cai

State Key Laboratory of Separation Membranes and Membrane Processes/National Center for International Joint Research on Separation Membranes; School of Materials Science and Engineering, Tianjin Polytechnic University, Tianjin 300387, China, Tel. +86 22 83955786, email: tjputll@163.com (L. Tan), hannapolyu@aliyun.com (N. Han), 913765833@qq.com (L. Zhang), cuizheyhh@163.com (Z. Cui), hiweilee@gmail.com(W. Li), zhangpolyu@aliyun.com(X. Zhang), 89318696@qq.com (J. Cai)

Received 7 October 2017; Accepted 6 May 2018

ABSTRACT

In this study, a melt processable poly(acrylonitrile-co-methyl acrylate)(P(AN-MA)) copolymer was used as membrane matrix, caprolactam (CPL) and glyceryl triacetate (GTA) were used as an eco-friendly mixed diluent. P(AN-MA) membranes with inter-connected sponge structure and porous surface were successfully fabricated via thermally induced phase separation (TIPS). The optimum ratio of CPL/GTA in the mixed diluent was 1:1 wt.%. Even though the concentration of P(AN-MA) was up to 25 wt.%, the surface of membrane still exhibited microporous structure. When the concentration of P(AN-MA) was 15 wt.%, the membrane formed in 20 °C air bath showed the highest water flux of 6802 L/m²h. With the increasing of copolymer content or cooling rate, the pore size decreased. In addition, all of the P(AN-MA) membranes exhibited a rejection to carbon ink more than 90 wt.%. The average pore size of the membranes was less than 270.5 nm, and the tensile strength was more than 2.8 MPa. It is anticipated that the facile and green technology TIPS will bring the P(AN-MA) membrane a step closer for practical applications, including clean-up of oil spills, waste water treatment, fuel purification, and separation of commercially relevant emulsions.

Keywords: Poly(acrylonitrile-co-methyl acrylate); Membranes; Thermally induced phase separation; High flux; Rejection

1. Introduction

Thermally induced phase separation (TIPS) is one of the most important methods to fabricate microfiltration and ultrafiltration polymer membranes [1–6]. Cui et al. [7] summarized the preparation of flat sheet and hollow fiber membranes via TIPS from 1990 to 2012. Compared with non-solvent induced phase separation (NIPS), TIPS is a green method for preparing porous membranes, which is driven by thermal transfer and can be controlled and adjusted easily. In the TIPS process, a homogeneous solution is obtained above the melting temperature (T_m) of the polymer with a diluent. Then, the solution is cooled down or quenched to induce phase separation. By changing the thermal transfer rate or solidification path of the homogeneous solution, various pore structures could be obtained, such as bi-continuous, cellular, needle-like, and vertically oriented structures [8–12]. Meanwhile, the TIPS method was applied to fabricate a variety of polyolefin polymer membranes, such as high-density polyethylene [1] and ultrahigh molecular weight polyethylene [13], which can't be dissolved in common solvents.

Polyacrylonitrile (PAN) is an important membrane material owing to its good thermal stability, good chemical resistance and mechanical properties [14–20]. It has been widely applied in water treatment, protein purification and juice clarification. Moreover, the nitrile groups of PAN could be modified and functionalized easily [21–22]. Hence, the modified and functionalized PAN-

*Corresponding author.

based membranes offer effective solution to enhance PAN membranes' biocompatibility and hydrophilicity by introducing reactive groups for further chemical reaction [19,20,23]. However, present PAN membranes were mainly fabricated via NIPS method, lots of organic and toxic solvents were needed, which exhibit typical finger-like pores. NIPS method is mainly applied for preparing PAN ultrafiltration membrane, comparatively, there are fewer microporous PAN membranes reported. Due to its special microstructure, the PAN-based copolymer is non-melting and non-soluble as a result. Compared with polyvinylidene fluoride, polystyrene, and polysulfone membranes, there are only few reports on PAN membranes fabricated via TIPS. Until 2012, Wu et al. [5,6,24] reported the fabrication of PAN membranes via TIPS method for the first time. They used dimethyl sulfone (DMSO2) and glycerol or polyethylene glycol (PEG) with different molecular weights as the mixed diluent. PAN porous membranes with cellular-like, sheet-like or needle-like porestructure were obtained via TIPS. In 2016, they successfully prepared PAN membranes with vertically oriented pores by changing the solidification pathway based on previous studies [12]. Because of the strong dipolar interaction between –CN groups, a dense membrane skin and closed or semi-closed pores incline to form in the process of TIPS. Now, the greatest challenge is to select an appropriate diluent to dissolve PAN at high temperature, which then promotes phase separation to take place with the thermal transfer.

In this study, in order to solve the problems described above and improve the thermal stability, flexibility and permeability of PAN membranes fabricated via TIPS, a flexible co-monomer, i.e., methyl acrylate (MA), was incorporated in the polymerization step [25,26]. A man-made melt processable poly(acrylonitrile-methyl acrylate) copolymer (P(AN-MA)) and a new eco-friendly mixed diluent composed of caprolactam (CPL) and glyceryl triacetate (GTA) were used to further optimize the structure of P(AN-MA) microporous membrane. A systematic study was performed to investigate the effects of CPL and GTA content, P(AN-MA) concentration and cooling rates on the pore shape, size, and porosity, as well as the pure water flux (PWF) and mechanical properties of P(AN-MA) microporous membranes.

2. Experimental

2.1. Materials

P(AN-MA) copolymer was synthesized by emulsion polymerization in our lab based on previous reports [30,31] (AN/MA mole ratios: 80/20; M_w = 5.6 × 10^5; T_m = 150~180 °C; T_d = 317~325 °C). Caprolactam (CPL, 99%), glyceryl triacetate (GTA, 98%) and N-methy-2-pyrrolidone (NMP, 98%) were purchased from Aladdin Industrial Corporation, and the chemical formulas are shown in Fig S1. PAN (Mη = 50,000 g/mol) came from Anqing Petroleum Chemical Corporation of China. Carbonic ink was provided by Shanghai Hero Ink Factory. De-ionized (DI) water was obtained from a Millipore MilliQ system. The P(AN-MA) copolymer and PAN polymer were dried before use, and other chemicals were used without further purification.

2.2. Preparation of P(AN-MA) and PAN membranes

The compositions and preparation conditions of P(AN-MA)/CPL/GTA membranes are listed in Table 1. The mixture was heated at 140 °C and stirred sufficiently to form a homogeneous solution under nitrogen atmosphere. After degassing the air bubbles, the solution was quickly poured onto a pair of clean quartz glass molds (200 × 200 mm) to form a film (thickness ~ 150 μm). Then, the mold was placed into an oven at 140 °C for 5 min, and immediately immersed in a cooling bath (air or water bath at 20 °C) to induce the homogeneous solution to phase separate until the solution became solid. When the nascent membrane was totally solidified, it was taken out of the mold, and the as-prepared membranes were placed into 20 °C deionized water and ethyl alcohol bath to extract the diluent solvents. PAN membrane was prepared by NIPS method with 15 wt.% PAN and 85 wt.% NMP.

2.3. Cloud point and viscosity measurement of P(AN-MA)/CPL/GTA system

The cloud point (T_{cloud}) was visually determined by observing the appearance of turbidity during the cooling process under an optical microscope (Olympus, BX51, Japan). The solid P(AN-MA)/CPL/GTA samples were cut into pieces and placed between a pair of microscope cover slips. The edges of the bottom microscope cover slip were sealed with a Teflon ring to prevent diluent loss. It was heated to 140 °C at a rate of 20 °C/min, maintained for 3 min, and then cooled down to 25 °C at a rate of 5 °C/min.

The crystallization temperature (T_c) and melting temperature (T_m) of P(AN-MA) in the casting solution were measured by a differential scanning calorimeter (Model DSC200F3, Netzsch, Germany). 5~8 mg samples were weighed and placed into a DSC pan. The sample was heated from 20 °C to 140 °C at a steady rate of 20 °C/min and main-

Table 1
Preparation condition of P(AN-MA) membranes

Sample number	Sample	P(AN-MA) concentration (%)	CPL mass fraction in the mixed diluent (%)	Cooling bath (°C)
1	15P(90C10G)	15	90	20
2	15P(80C20G)	15	80	20
3	15P(70C30G)	15	70	20
4	15P(60C40G)	15	60	20
5	15P(50C50G)	15	50	20[a]
6	18P(50C50G)	18	50	20[a]
7	20P(50C50G)	20	50	20[a]
8	22P(50C50G)	22	50	20
9	25P(50C50G)	25	50	20
10	30P(50C50G)	30	50	20

[a]The cooling medium isboth air andwater bath at 20 °C, while the others are air bath at 20 °C.
The ingredients are denoted as xP(yCzG), where P, C and G represent P(AN-MA), CPL and GTA, respectively.

tained for 2 min to eliminate the thermal history, cooled down from 140 °C to –20 °C at 10 °C /min and then reheated to 140 °C at 10 °C/min under the protection of a nitrogen atmosphere. The DSC of 15P(50C50G) homogeneous was also measured at different heating and cooling rate. The T_m and T_c were taken as the peak temperature of the resulting endothermic and exothermic peaks of P(AN-MA) in the casting solution, respectively, in the second heating curve.

The viscosity of the P(AN-MA)/CPL/GTA ternary system was determined by Thermo Scientific HAAKE MARS, Germany. The temperature was scanned from 160 °C to 80 °C and the cooling rate was 10 °C /min.

2.4. Membrane morphology

A dry P(AN-MA) flat membrane was frozen and fractured in liquid nitrogen to obtain a tidy cross-section. Then, the samples were sputtered with gold using a sputter coater (SCD-005), and the surface and cross-sectional morphologies were imaged by FESEM (Hitachi S-4800, Hitachi, Japan) at an acceleration voltage of 10.0 kV.

2.5. Porosity and pore size measurement

The porosity is defined as the volume of pores divided by the total volume of the membrane [27]. A wet P(AN-MA) membrane was weighed immediately after removing the superficial water with filter paper. Then, the same membrane was weighed again after it was dried in a vacuum oven for 24 h at 20 °C. Every membrane was tested at least five times. The porosity (P) was calculated by the following formula:

$$P = \frac{(m_1 - m_2)/\rho_{water}}{(m_1 - m_2)/\rho_{water} + m_2/\rho_{AN-MA}} \times 100\% \quad (1)$$

where ρ_{water} and $\rho_{AN\text{-}MA}$ are the densities of water and P(AN-MA), respectively, m_1 is the wet membrane weight, and m_2 is the dry membrane weight. $\rho_{AN\text{-}MA}$ was obtained by the weighing method. The AN-MA copolymers in powder form were placed in a circular mold formed by stacking multiple layers of iron sheets. The powders in the mold were compressed under pressure. The average thickness and diameter of the samples were measured by a screw micrometer, and at least three specimens were tested for accuracy.

The pore size and pore size distribution were measured by the nuclear magnetic method (PDNMR20-015V, Suzhou Niumag Analytical Corporation).

2.6. Pure water permeability

The membrane samples were cut into rounded shapes (available surface area is 4.9 cm^2). The pure water flux (PWF) of the membranes was determined on a homemade device with a pressure-driven test cell. First, the membranes were pre-wet with pure water and pre-pressurized at 0.12 MPa 25 °C for 0.5 h. Then, the transmembrane pressure was reduced to 0.10 MPa for operation at a steady-state water flux with less than 2% deviation. Each sample was tested at least five times, and the average number was taken as the final value. The PWF (J_w) was defined by the following formula:

$$J_W = \frac{V}{A \times \Delta t} \quad (2)$$

where J_w is the PWF (L/m^2·h), V is the volume of permeated water (L), A is the available membrane area (m^2) and Δt is the permeate time (h).

2.7. Theink rejection

The rejection experiment used the same apparatus as the water flux measurement. The membranes were pre-pressurized at 0.1 MPa at 20 °C for 10 min. The ink rejection of the membrane was determined with 0.3 g/L carbonic ink solution. The average size of carbonic black was 0.17 μm. The filtrate solution concentration was determined using a SHIMADZU UV-2000 (Thermo, USA) spectrometer, at a fixed wavelength of 228 nm.

The rejection rate (R) of the membrane was calculated by the following equation:

$$R(\%) = \left(1 - \frac{C_1}{C_0}\right) \times 100 \quad (3)$$

where C_1 and C_0 are carbonic ink concentrations in the filtrate and feed solution (g/L), respectively. C_0 = 0.3 g/L and C_1 was the carbonic ink concentration of the filtrate solution.

2.8. Tensile strength

The tensile strength of the samples was measured by a tensile testing machine (CMT4503, Meitesi Industry Co. Ltd, China). The samples were cut into rectangular shapes (40 × 10 mm). A testing speed of 10 mm/min at 20 °C was utilized. The membrane was fixed vertically between two pairs of clamps with a test length of 20 mm. The thickness was measured by an electronic digital readout micrometer (0–25 mm/0.001, Shanghai Zijiu Measuring Tool Co., Ld, China). The reported values represent the average of at least five samples.

3. Results and discussion

3.1. Solubility parameters analysis

The solubility parameter δ is a very important parameter for analyzing the solubility of polymer insolvent or the miscibility between solvent and polymers [30]. The overall solubility parameter (δ) includes the dispersion force component (δ_d), polar component (δ_p), and hydrogen bonding component (δ_h). In addition, $\Delta\delta_{12}$ is used to calculate the interaction between two chemicals. A smaller value of $\Delta\delta_{12}$ indicates a better compatibility between the polymer and the solvent. The various solubility parameters are listed in Table 2. Hansen's parameters δ, δ_{12} can be directly calculated using the following equations:

$$\delta^2 = \delta_d^2 + \delta_p^2 + \delta_h^2 \quad (4)$$

$$\Delta\delta_{12} = \left[(\delta_{d1} - \delta_{d2})^2 + (\delta_{p1} - \delta_{p2})^2 + (\delta_{h1} - \delta_{h2})^2\right]^{1/2} \quad (5)$$

Table 2
Solubility parameters of typical solvents forPAN and P(AN-MA) copolymer

Chemicals	δ_d(MPa$^{0.5}$)	δ_p(MPa$^{0.5}$)	δ_h(MPa$^{0.5}$)	δ (MPa$^{0.5}$)	$\Delta\delta_{12}$ (MPa$^{0.5}$)	Ref.
P(AN-MA)	19.49	10.77	8.26	23.75		[32]
CPL	19.30	10.00	11.60	24.60	11.78	[34]
Ethylene carbonate (EC)	15.46	14.34	10.96	23.76	36.28	[32]
Dimethyl sulfone ($DMSO_2$)	19.00	19.40	12.30	29.90	91.04	[35]
N,N-dimethyl-formamide (DMF)	17.40	13.70	11.30	24.80	22.19	[36]
Dimethyl sulfoxide (DMSO)	18.40	16.40	10.20	26.70	36.65	[36]
γ-Butyrolactone (γ-BA)	19.00	16.60	7.40	26.29	34.97	[33]
GTA	16.50	4.50	9.10	19.37	48.96	[37]
Dimethyl acetamide (DMAC)	16.80	11.50	10.20	22.77	11.53	[33]
Propylene carbonate (PC)	20.20	18.00	4.10	27.22	69.84	[28]

δ, δ_d, δ_p, and δ_h are the overall solubility, dispersion, polar and hydrogen parameters, respectively.
$\Delta\delta_{12}=[(\delta_{d1}-\delta_{d2})^2+(\delta_{p1}-\delta_{p2})^2+(\delta_{h1}-\delta_{h2})^2]^{1/2}$, where 1 and 2 denote P(AN-MA) and solvent, respectively.

The solubility parameters of P(AN-MA), CPL, GTA and other solvents reported in the literatures are shown in Table 2. PAN is a polar polymer,therefore,only polar solvents exhibit good compatibility with it, such as DMSO, DMSO2, DMF, EC, γ-BA, DMAC [33], and PC [34].

PAN can't melt, while the melt processable matrix P(AN-MA) copolymer could be melt processed at 180–220 °C [25,26] and possesses no polar solvent was needed in the preparation process. What's more, the polar component (δ_p) decreased from 16.20 MPa$^{0.5}$ (PAN) to 10.77 MPa$^{0.5}$ (P(AN-MA)). It is indicated that the P(AN-MA) copolymer could be dissolved in a solvent with lower polarity. Among the common solvents of PAN, such as EC, DMSO2, DMF, DMSO, DMAC and PC, the $\Delta\delta_{12}$ between CPL and P(AN-MA) (11.78 MPa$^{0.5}$) is close to the minimum value derived from the polar solvent and the copolymer. It is worth noting that CPL is crystal form at room temperature, which can promote the phase separation of ternary system via TIPS. Therefore, CPL was selected as the solvent to dissolve the P(AN-MA) copolymer in this study. A low value of $\Delta\delta_{12}$ is better for improving the compatibility of copolymers and solvents, while the high value of $\Delta\delta_{12}$ is better for L-L phase separation and forms bi-continuous networks, cellular-, spongy- or branch-like morphology as expected. Hence, the non-solvent GTA was used as an additive to adjust the $\Delta\delta_{12}$ value (between P(AN-MA) and mixed diluent) from 11.78 MPa$^{0.5}$ to 18.06 MPa$^{0.5}$ as listed in Table 3. It means that the compatibility and phase separation process of ternary system could be adjusted by controlling the content of CPL or GTA (Fig. S4).

Table 3
Solubility parameter of the mixed diluent

Mixed diluent (mass ratio CPL/GTA[a])	δ_d (MPa$^{0.5}$)	δ_p (MPa$^{0.5}$)	δ_h (MPa$^{0.5}$)	$\Delta\delta_{12}$ (MPa$^{0.5}$)
100/0	19.30	10.00	11.60	11.78
90/10	19.50	9.51	11.38	11.52
80/20	18.80	9.02	11.15	11.89
70/30	18.54	8.51	10.92	13.09
60/40	18.27	7.98	10.68	15.13
50/50	18.00	7.44	10.44	18.06

[a]Calculated result according to ref [40]. Where 1 and 2, respectively, denote the polymer and mixed diluent.

3.2. Phase diagram of P(AN-MA)/CPL/GTA systems

The phase diagram gives important information for adjusting the phase separation process in the TIPS method. The DSC curves of P(AN-MA)/CPL/GTA ternary system with various P(AN-MA) and CPL contents are shown in Fig. S2. All of the DSC curves exhibited only one peak in the heating or cooling process. It is indicated that CPL is a good solvent for P(AN-MA) copolymer, which is consistent with the theoretical analysis shown in 3.1. According to Flory–Huggins solution thermodynamics, the T_m, and T_c would be depressed in the ternary system with mixed diluent content [4]. Moreover, at room temperature, CPL and P(AN-MA) are solids, while GTA is a liquid solution. So, with the increase of the concentration of GTA, the initial T_m and T_c further moved to lower temperatures. When P(AN-MA) concentration was kept at 15 wt.%, the GTA concentration increased from 10 wt.% to 50 wt.% in the mixing diluent. The initial T_m of P(AN-MA)/CPL/GTA ternary system decreased from 66.8 °C to 48.8 °C and the initial T_c dropped from 26.1 °C to –4.8 °C. Fig. 1 shows the changing trend of the initial phase separation and crystallization temperature of various P(AN-MA) membranes. The interaction between P(AN-MA) copolymer and GTA is lower than that of the copolymer with CPL. It is shown that (48.96 MPa$^{0.5}$), corresponding to the interaction force between the copolymer and GTA is higher than that of P(AN-MA) with CPL, i.e., (11.78 MPa$^{0.5}$). With the GTA content increasing, the interaction force between P(AN-MA) and mixed diluent CPL/GTA decreased, the initial phase separation temperature T_{cloud} increased as expected [5]. When the GTA content changed in the range of 10 wt.%–50 wt.% in the mixed diluent, T_{cloud} increased from 90 °C to 135 °C and T_c of the ternary system dramatically decreased from 26.1 °C to –4.8 °C. Because the compatibility between P(AN-MA) and CPL becomes poor with the addition of GTA, T_{cloud} shifts to the high-temperature region. T_{cloud} and T_c are generally

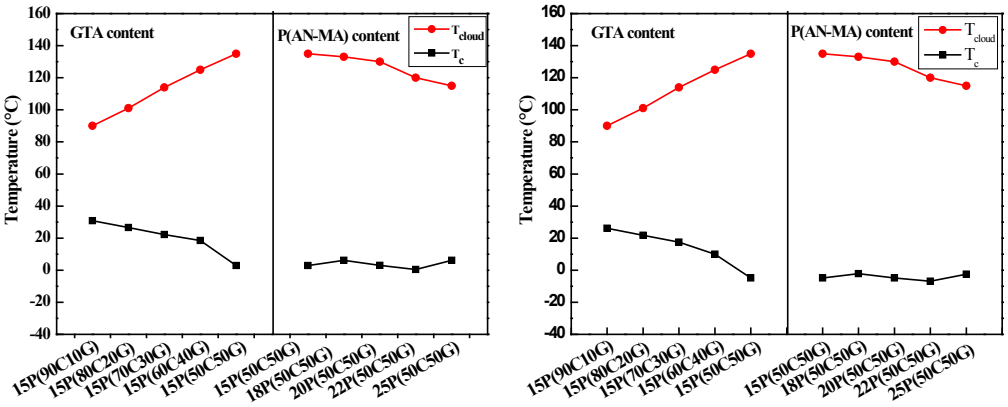

Fig. 1. Phase diagram of the P(AN-MA)/CPL/GTA ternary system with various P(AN-MA) and CPL contents: the solid circles (•) indicates the cloud points (T_{cloud}) and solid squares (■) indicates the dynamic crystallization temperatures (T_c).

assumed to be the upper and bottom boundary of L-L phase separation region, respectively [5]. The enlarged phase separation intervals offer enough L-L separation regions. It means that the liquid droplets had longer growth time at a constant cooling rate.

Based on our experiment results, as shown in Fig. 2, the 15P(50C50G) ternary system could be kept thermally stable in a 20 °C air bath. To obtain a porous membrane with an ideal pore structure, the formation temperature of 20 °C was adopted in this study.

3.3. Effects of GTA content on the morphology of membranes

Fig. 3 presents the surface and cross-section morphologies of membranes formed in 20 °C air bath. The cross-section of the 15P(AN-MA) membrane deformed and wrinkled obviously, when GTA content was lower than 20 wt.% in the mixed diluent. This structure implied that the membrane has poor non-deformability in the following drying and applying process. The 15P(80C20G) membrane exhibited dense cross-section and surfaces, as shown in Figs. 3c and d. It is ascribed to the strong interactions between the P(AN-MA) copolymer and mixed diluent. This result was also consistent with Fig. 1. There was narrow L-L phase separation region for the ternary system, when GTA content was as low as 20 wt.%. While, the surface morphology of the P(AN-MA) membrane changed from a dense skin to a porous structure,when the GTA content increased from 30 wt.% to 50 wt.%. The cross-sections of 15P(60C40G) and 15P(50C50G) samples exhibited a uniform spongy structure, as shown in Fig. 3b. It was due to the weak interactions between the P(AN-MA) copolymer and mixed diluent with GTA content increasing, and ternary system had enough L-L separation regions.

The membrane pore size mainly depends on the viscosity of the initial phase separation and L-L phase separation regions. A lower viscosity and a wider L-L phase separation region are better for increasing the pore size [5]. Fig. 4 shows the viscosity relationship curves of P(AN-MA)/CPL/GTA ternary system and GTA content in mixed diluents at different temperatures. When the GTA content increased from 10 wt.% to 50 wt.%, the viscosity corresponding to the initial phase separation decreased from

Fig. 2. Apparent state of 15P(50C50G) solution in 20 °C air bath.

0.156 Pa·s to 0.130 Pa·s. Meanwhile, the temperature corresponding to the initial phase separation increased from 90 °C to 135 °C. With the GTA content increasing, the viscosity of the initial phase separation decreased, L-L phase separation regions increased as a result. Those offered a higher probability for droplets growth. It can be seen in Fig. 3, the surface morphology of the P(AN-MA) membrane changed from a dense skin to porous structure.

3.4. Effect of P(AN-MA) concentration on the morphology of membranes

Polymer concentration is another crucial factor to influence the resulting morphologies of membranes. Figs. 5a–d present the morphologies of P(AN-MA) membranes prepared with 15–30 wt.% of P(AN-MA), and kept GTA content constant at 50 wt.% in the mixed diluent.

Wu et al. [5] reported that the decrease in pore size is mainly related to the increase of viscosity of the polymer

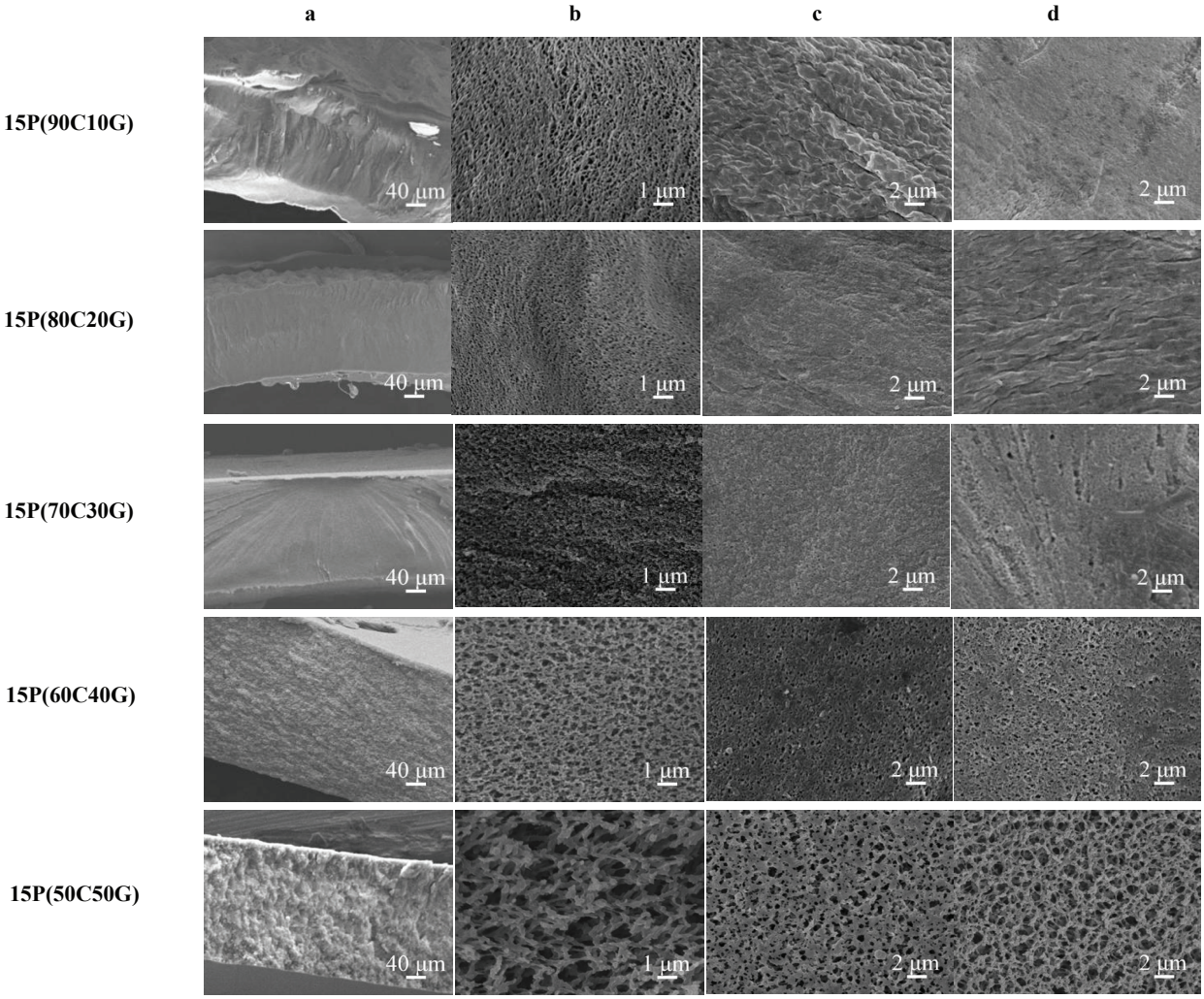

Fig. 3. SEM images of 15P(AN-MA) membranes formed in 20 °C air bath: (a) cross-section (250×), (b) enlarged cross-section (10 000×), (c) top surface(5000×), and (d) bottom surface(5000×). (The GTA content in the mixed diluent ranged from 10 wt.% to 50 wt.%).

solution. The size of surface pores dramatically decreased as the PAN concentration increased. It was shown that the apparent viscosity increased 5 times,when comparing PAN concentration of 21 wt.% with 15 wt.%. A similar trend was also reported by other papers [36,37]. In this work, the P(AN-MA) solution also exhibited the same trend as expected. Under the same temperature, the viscosity of the P(AN-MA)/CPL/GTA ternary system increased obviously with the increase of P(AN-MA) content, as shown in Fig. 6. The pore size also exhibited the same trend as other papers, the pore size decreased obviously with P(AN-MA) content. The changing trend of pore size in this work is same as that reported in previous paper [4–6]. With the P(AN-MA) content increasing, the pore size of skin and cross section all decreased obviously, which decreased from 270.5 nm to 73.0 nm with P(AN-MA) content changed from 15 wt.% to 30 wt.%.

In this study, all of the cross-sections of the xP(50C50G) membrane exhibited a spongy porous structure, as the P(AN-MA) concentration increased from 15 wt.% to 25 wt.%. Similarly, the pore size decreased with the increase of

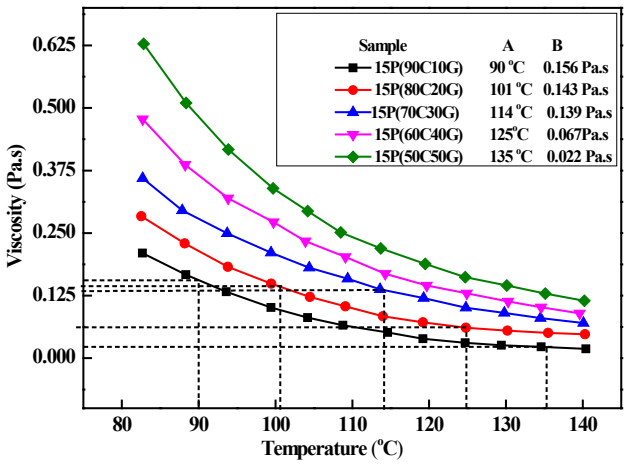

Fig. 4. The relationship curves of the viscosity of P(AN-MA)/CPL/GTA ternary system and temperatures; initial phase separation temperature (column A) and the viscosity corresponding to the initial phase separation temperature (column B).

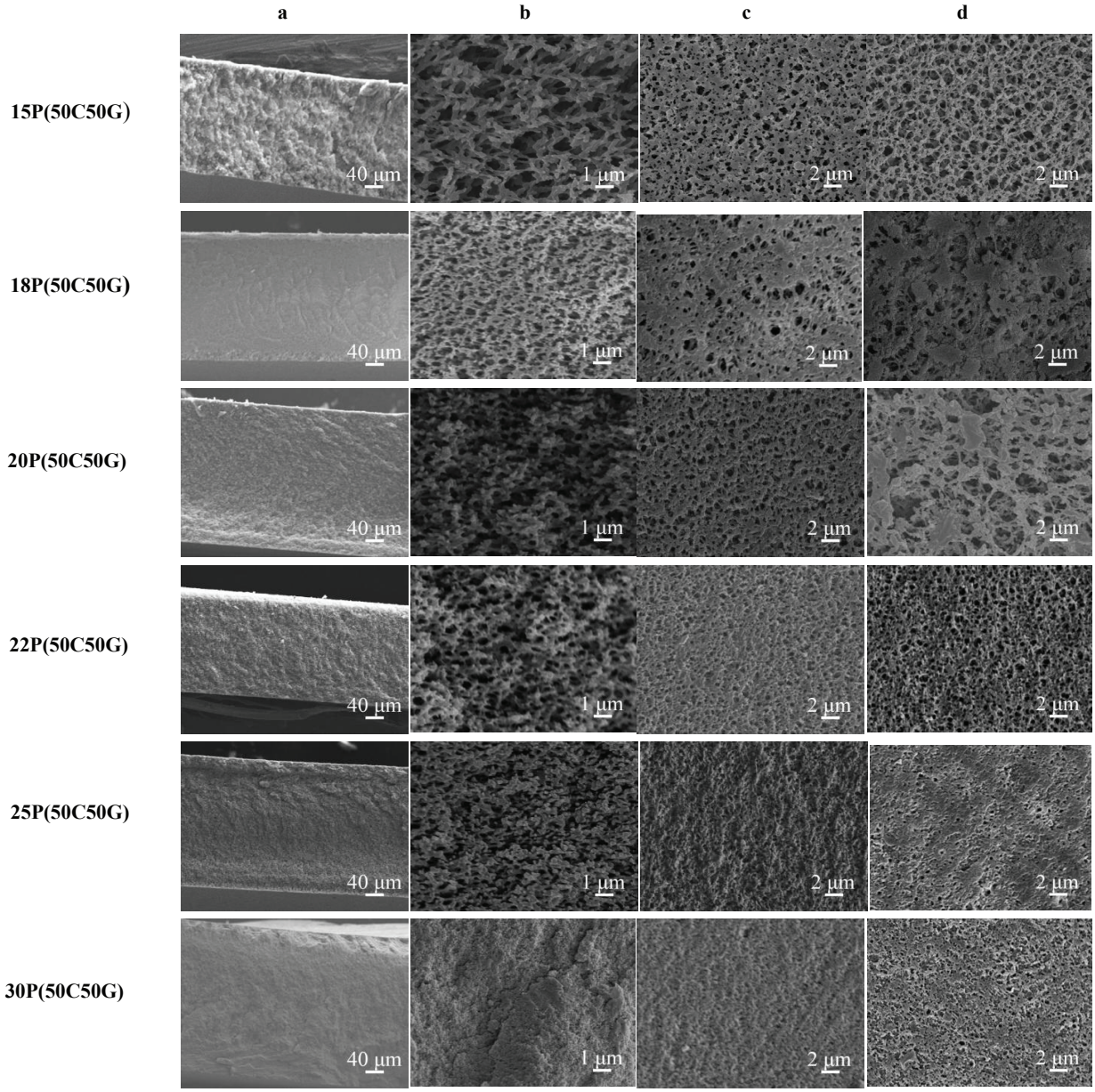

Fig. 5. SEM images of P(AN-MA) membranes prepared with 50 wt.% GTA in the mixed diluent: (a) cross-section (250×), (b) enlarged cross-section (10 000×), (c) top surface (5000×), and (d) bottom surface (5000×). The P(AN-MA) content in the ternary system ranged from 15 wt.% to 30 wt.%. (20 °C air bath).

P(AN-MA) concentration. The morphology of the cross-section and surface became dense and non-porous as the P(AN-MA) concentration was up to 30 wt.%. In contrast, 15 wt.% P(AN-MA) had a larger pore size. Because of the liquid droplets in the ternary system with a lower viscosity went through a longer growth period, and a larger pore size was obtained as a result.

3.5. Effect of cooling rate on the morphology of membranes

The effects of cooling rate on T_c and T_m of the 15P(50C50G) casting solution are shown in Fig. 7 and Table S1. The cooling rate had a remarkable influence on i) T_c, which decreased as the cooling rate increased and ii) the liquid droplets growth period. A higher T_c is better for membrane formation via TIPS at room temperature. Hideto Matsuyama thought that cloud points were independent of the cooling rate [37]. Thus, it is can be seen that the L-L phase separation region was changed only by the dynamic crystallization temperatures when the cooling rate changed.

It can be seen that the T_c of the samples decreased progressively with the increase of cooling rate. The L-L separation regions were enlarged before the crystallization of samples, but the droplet growth period was shortened obviously. The initial T_c value corresponding to the differ-

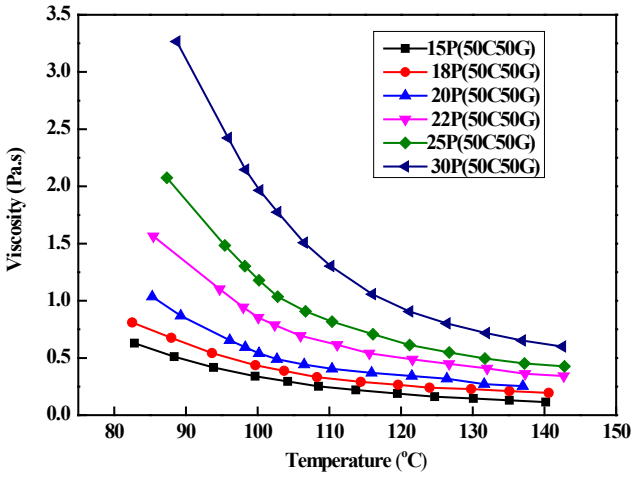

Fig. 6. Relationship curves of the viscosity of P(AN-MA)/CPL/GTA ternary system and environmental temperatures.

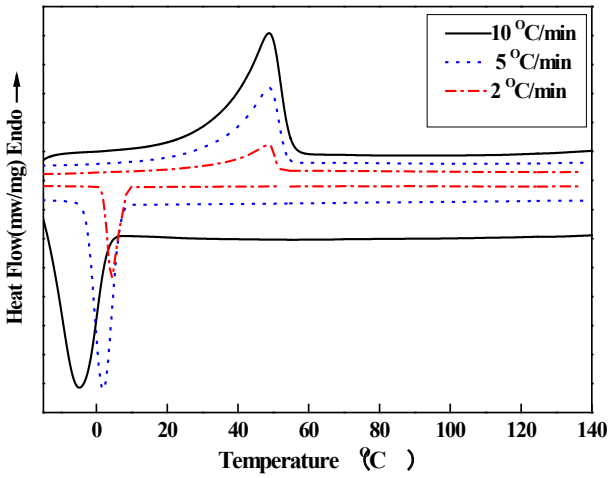

Fig. 7. Crystallization and melting behaviors of 15P(50C50G) casting fluid at different cooling rates. The solid lines represent 10 °C/min, dot lines represent 5 °C/min, and dash dot lines represent 2 °C/min.

ent cooling rates of 2 °C/min, 5 °C/min and 10 °C/min were 4.2 °C, 1.9 °C and –4.8 °C. For example, when the 15P(50C50G) solution decreased from the homogeneous solution temperature (140 °C) to the onset point of T_c, it only required 14.5 min at a heating rate of 10 °C/min, while it required 67.9 min for the sample to start crystallizing at a cooling rate of 2 °C/min. The lower cooling rate, the longer liquid droplets growth period. Meanwhile, the viscosity of P(AN-MA)/CPL/GTA solution obviously depends on the environmental temperature, which increases obviously with decreasing temperature, as seen in Figs. 4 and 6. Therefore, a lower cooling rate is better for prolonging the growth period of liquid droplets and depressing the increasing rate of solution viscosity. Both are highly effective for further enhancing the liquid droplet growth period and perfecting the membrane pore size.

SEM images of P(AN-MA) membranes are shown in Fig. 8, which are prepared with 15 wt.%, 18 wt.% and 20 wt.% P(AN-MA) and formed in 20 °C water bath. Comparing the membranes shown in Fig. 8 with that shown in Fig. 5, the membranes formed in an air bath possessed better interconnectivity and larger pore size. The average pore sizes of the 15P(50C50G), 18P(50C50G) and 20P(50C50G) membranes are 270.5 nm, 155.2 nm and 144.8 nm, respectively, which are summarized in Table S2. The corresponding pore sizes of membranes formed in the 20 °C water bath are 153.4 nm, 117.6 nm and 102.3 nm, respectively. Because of the thermal capacity of water is higher than that of air. With the increase of cooling rate (water as the coagulation bath), the homogeneous solution would undergo a short and weak L-L phase separation, the pore size in the cross-section decreased. A slower cooling rate leads to a longer coursing period due to the low temperature gradient and vice versa, which is better for forming an interconnecting pore structure.

3.6. The pore sizes and distribution, permeability and porosity of membranes

Fig. S5 shows the pore size distribution of P(AN-MA) membranes prepared with various polymer concentrations. Fig. S6 exhibits the pore size distribution of P(AN-MA) membranes formed by different cooling rates respectively. It can be seen that the pores were composed of both small pores and large pores. Most of the pore size was higher than 100 nm. Thus, the average pore size was recognized as the average value of pores. When the P(AN-MA) concentration increased from 15 wt.% to 30 wt.%, the average pore size in the cross section decreased from 270.5 nm to 72.3 nm, and the pore size distribution regions obviously became narrow, shown in Fig. 10. It is attributed to the higher viscosity and the narrow L-L phase separation region for the ternary system containing 30 wt.% P(AN-MA). With the increase of cooling rate, as shown in Fig. 11, the pore size decreased,and the distribution became narrower. Taking 15P(50C50G) membrane as an example, the pore size distribution decreased from 117.6–410.3 nm to 83.1–204.9 nm, when the coagulation bath changed from 20 °C air bath to 20 °C water bath. It is ascribed to a short liquid drop growth period at a higher cooling rate. T_{cloud} and T_c are generally assumed to be the upper and bottom boundary of liquid drop growth period. At a constant ternary system, the gap of T_{cloud} and T_c is certain. The growth period of droplet is mainly decided by the cooling rate. Because water has a high thermal capacity, the cooling rate in water is bigger than that in air. As a result, the pore size of membranes decreased obviously with cooling rate increasing. Thus, it is feasible to obtain an ideal pore structure of P(AN-MA) membrane by adjusting the polymer concentration and cooling rate.

The permeability and porosity of P(AN-MA) porous membranes are shown in Fig. 9. Both the pore size and porosity increased with the increase of GTA content. The 15P(50C50G) membrane exhibited a good interconnected structure, larger pore size and high surface porosity, as shown in Fig. 3. The PWF of the 15P(50C50G) membrane was up to the maximum value of 6802 L/m²h. When the GTA content in the mixed diluent increased from 10 wt.% to 50 wt.%, the PWF and porosity increased from 268.2 L/m²h to 6802 L/m²h, and the porosity increased from 61.3 wt.% to 79.4 wt.%, respectively, due to its inter-connected

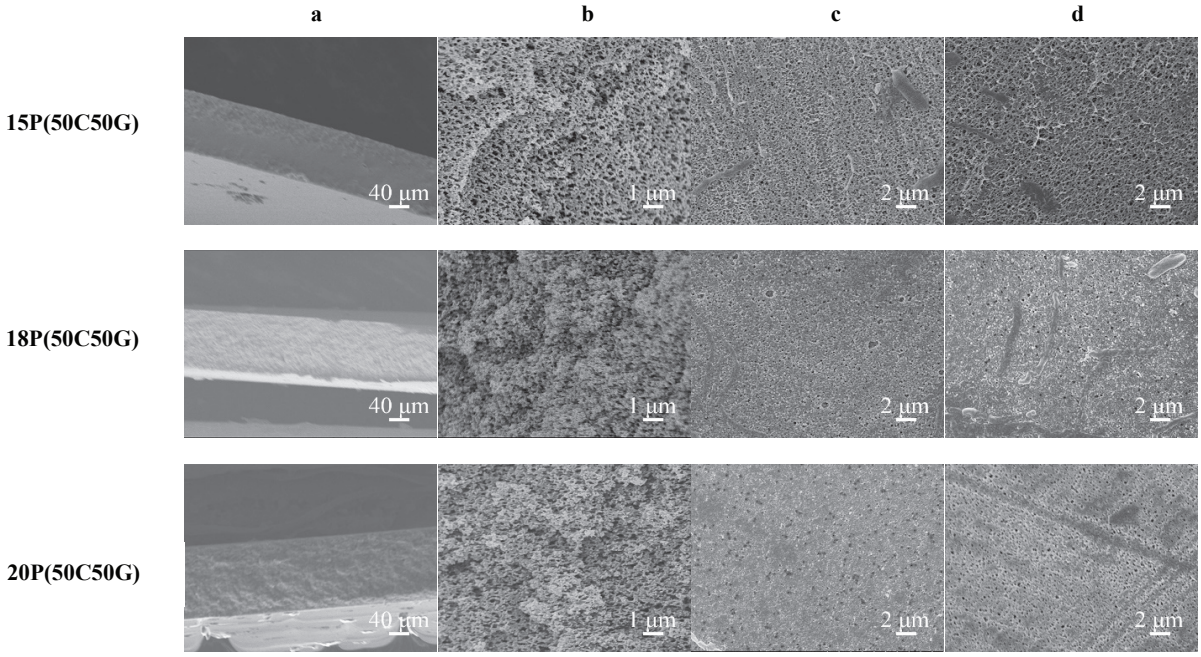

Fig. 8. SEM images of P(AN-MA) membranes prepared with 15 wt.%, 18 wt.% and 20 wt.% P(AN-MA): (a) cross-section (250×), (b) cross-section (10 000×), (c) top surface (5 000×), and (d) bottom surface (5 000×). The mixed diluent was composed of CPL/GTA (50/50 wt.% at 20 °C in a water bath).

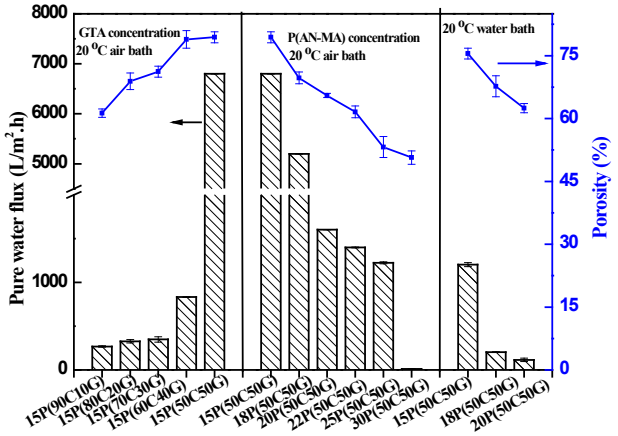

Fig. 9. Water flux (bars) and porosity (squares) of P(AN-MA) membranes prepared under various conditions.

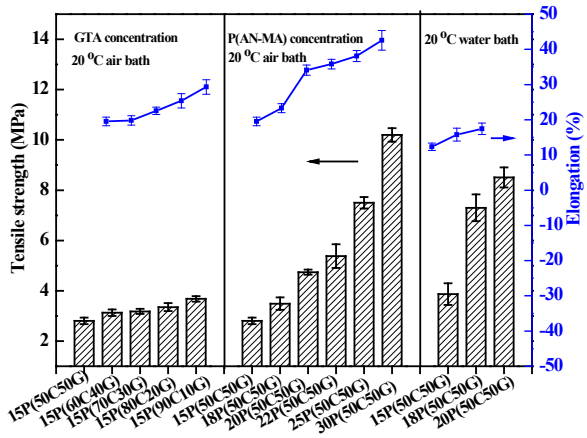

Fig. 10. Tensile strength of the wet P(AN-MA) membranes.

sponge structure and highly porous surface as shown in Fig. 3.While, the concentration of P(AN-MA) changed from 15 wt.% to 30 wt.%, the porosity of the membrane decreased from 79.4 wt.% to 50.7 wt.%, and the PWF decreased from 6802 L/m²h to 30 L/m²h, ascribed to the poor connectivity and tiny pores as mentioned above (Fig. 5 and Fig. S5).

The cooling rate is another crucial parameter to adjust the pore size and porosity. The permeability and porosity of P(AN-MA) porous membranes were depressed with the increase of cooling rate. Compared with the 18P(50C50G) membrane formed in the 20 °C air bath, the sample formed in the 20 °C water bath has a slight lower porosity, i.e., 69.7 wt.% vs. 67.7 wt.%.It is worthy to note that the PWF exhibited a dramatic depression from 5200 L/m²h to 204 L/m²h, when the coagulation bath was changed from the air to the water keeping the environmental temperature constant. The 15P(50C50G) and 20P(50C50G) membranes formed in the air bath and water bath showed similar changing trend.

3.7. The mechanical property and rejection of P(AN-MA) membranes

The mechanical strength and elongation are shown in Fig. 10. The wet membranes formed in the water bath had a better

tensile strength and elongation than those formed in the air bath. It was associated with the lower porosity and small pore size of the membrane formed in the waterbath [5,32]. With the increase of P(AN-MA) copolymer content, the permeability of the membrane gradually decreased until a dense skin appeared as the P(AN-MA) content up to 30 wt.% (Figs. 5 and 9). Advantageously, the tensile strength improved obviously from 2.8 MPa to 10.2 MPa and the elongation increased obviously from 19.54 % to 42.55 %, when the P(AN-MA) content increased from 15 wt.% to 30 wt.%, in the 20 °C air bath.

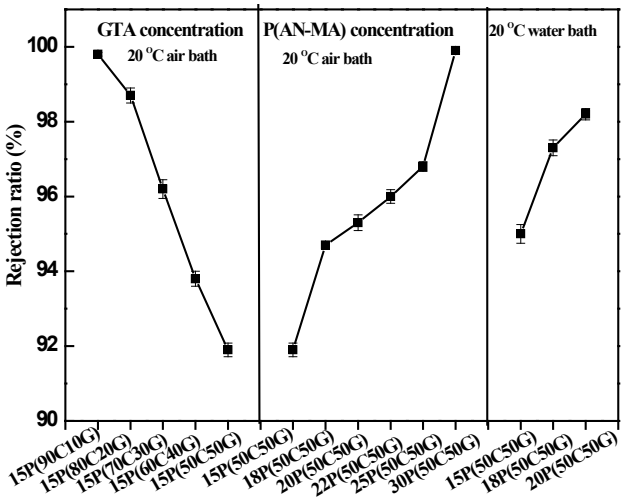

Fig. 11. The rejection of P(AN-MA) membranes.

Ji et al. [39] and Wanget al. [40] reported that the rejection of microfiltration membrane could be evaluated by using carbonic ink. The carbonic ink solution was comprised of nanocarbon particles with diameters from 60–450 nm (the average size is 170 nm), as shown in Fig. S3. The concentration of carbonic ink solution was set at 0.3 g/L in our experiments. The rejections of membranes are shown in Fig. 11. The sample of 18P(50C50C) membrane was used as a filtration and the separation effect was recorded by a photograph as shown in Fig. S4 and Table. S2, which summarizes some properties of the P(AN-MA) membranes fabricated in the air and water baths. It is evidenced that the rejection was a comprehensive performance of the membrane porosity, the inter-connectivity of the cross-section and the surface pore size.

The apparent morphology of PAN and P(AN-MA) wet membranes during the drying process (at 25 °C for 4 h) were also investigated, which are shown in Fig. 12. The P(AN-MA) membranes keep even and no wrinkle appearing as the GTA content higher than 20 wt.%. While, the PAN membrane can't keep even and wrinkle appearing, when it fabricated by NIPS method. It's due to the P(AN-MA) membrane possesses bi-continuous pore structure and avoid finger-like pore, when it formed via TIPS method, it is especially better for dry state preservation and transport.

A further comparison of PAN or PAN-based membranes reported in previous literatures via TIPS is presented in Table 4. The P(AN-MA) copolymer could be dissolved in the mixed

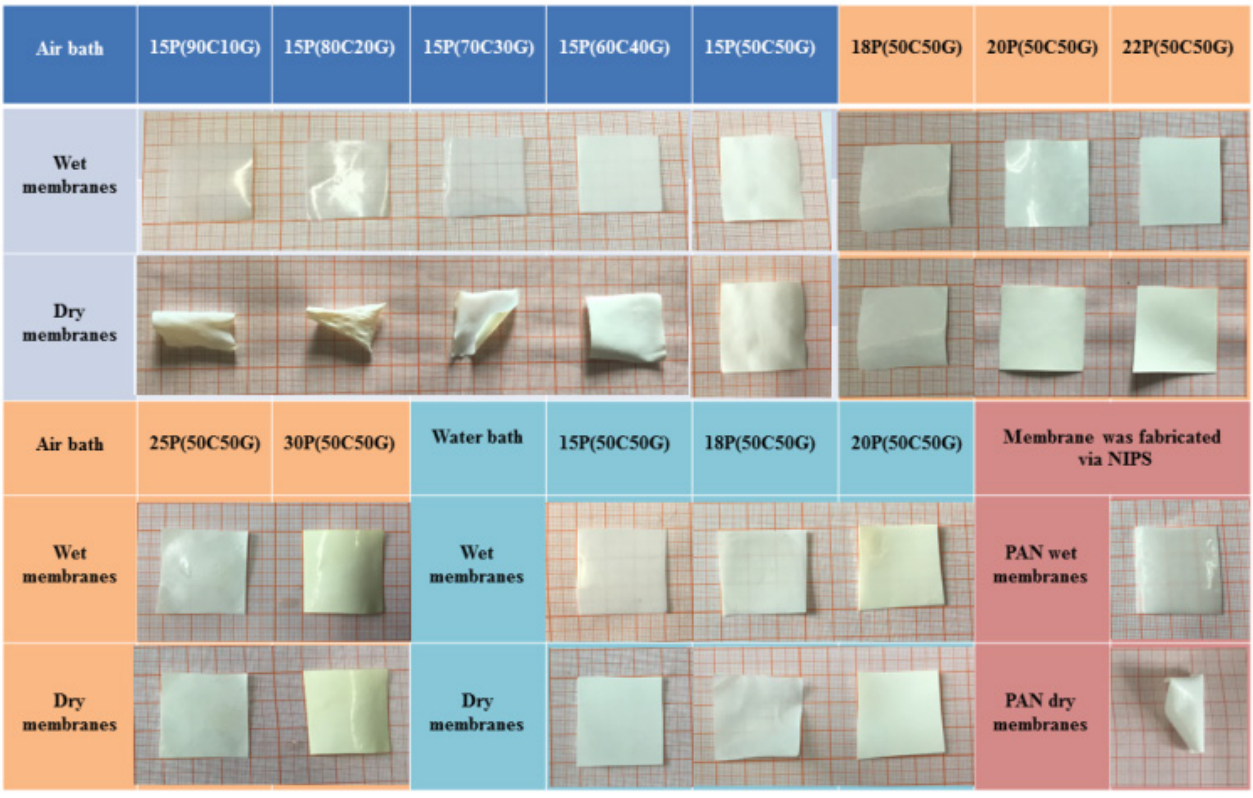

Fig. 12. The apparent morphology of P(AN-MA) and PAN wet membranes during the dry process, PAN membrane was fabricated by NIPS and P(AN-MA) membranes were fabricated by TIPS.

Table 4
Comparison of PAN and PAN-based membranes prepared via TIPS reported in the literature

Membrane composite	Fabricated temperature (°C)	Pore size (μm)	Porosity (%)	Rejection (%)[b]	Maximum pure water flux (L/m²·h)	Tensile strength (MPa)[c]	Ref.
PAN/$DMSO_2$/Glycerol	160	20.20/7.30[a]	87.5	N	3000	1.6	[5]
PAN/$DMSO_2$/PEG	160	N	83.7	N	1500	N	[29]
PAN/PEG/PVP	180	N		N	131	6.8	[46]
AN-MA/γ-BA/GTA	160	0.40	70.0	N	80	3.8	[11]
AN-MA/EC/TEC	160	2.40	76.0	N	66	4.6	[47]
AN-MA/CPL/GTA	140	0.27	79.4	91.9a	6802	2.8	This work

N ~ Not reported in the paper; the geometries of all membranes were flat sheets.
[a]Both the long and short diameter of oval-shaped pores.
[b]A carbonic black ink with a particle size of 0.17 μm was used as the specimen, and the concentration of the feed solution was 0.3 g/L.
[c]Wet membrane tensile strength.

diluent CPL/GTA at a lower temperature of 140 °C. There is a difference about 20–40 °C lower than that reported in the references. It has a great advantage in energy saving. Furthermore, the 15P(50C50G) membrane formed in 20 °C air bath had porous membrane surface and the smallest average pore size of 0.27 um. The carbonic ink with an average particle size of 170 nm could be filtered by 15P(50C50G) and the rejection up to 91.9%. It also possesses the best excellent permeabilty up to 6802 L/m²h. Therefore, the melt processable P(AN-MA) provides a new way to fabricate porous PAN-based micro-filtration membranes via TIPS.

4. Conclusion

In this study, a man made melt processable P(AN-MA) copolymer was used as membrane matrix, the solvent CPL and non-solvent GTA were used as a mixed diluent. A series of P(AN-MA) porous membrane was fabricated via TIPS method. The P(AN-MA) membranes exhibited inter-connected sponge structure and porous surface, when the content of GTA was up to 30 wt.% in 20 °C air bath. The optimum ratio of CPL/GTA in the mixed diluent was 1/1 wt.%. Even when the P(AN-MA) content was up to 25 wt.%, the surface still exhibited a porous morphology. The average pore size of 15P(50C50G) membrane was 270.5 nm. The rejection to carbonic ink with an average particle size of 170 nm was 91.9%. The P(AN-MA) membrane fabricated in 20 °C air bath had excellent permeability, which possess a PWF up to 6802 L/m²h and a porosity up to 79.4 wt.%, respectively. The pore size and rejection have opposite trend, pore size becomes larger with GTA content increase, P(AN-MA) concentration and cooling rate decrease.

The melt processable P(AN-MA)copolymer provides a new way to fabricate PAN-based micro-filtration membranes via TIPS. It also provides a reference for the formation of other semi-crystalline polymer membrane via the green technology of TIPS, especially for the polymer cannot be dissolved at room temperature.

Acknowledgments

The authors wish to thank the National Natural Science Fund of China (B060306); Postdoctoral Program projects (201402011); Tianjin Municipal Science and Technology Project (16YFZCSF00120) for financial support; Applied Basic Research and Frontier Technology Research Programs funded by Tianjin Municipal Science and Technology Commission (14JCYBJC19600).

References

[1] D.R. Lloyd, K.E. Kinzer, H.S. Tseng, Microporous membrane formation via thermally induced phase separation. I. Solid-liquid phase separation, J. Membr. Sci., 52 (1990) 239–261.
[2] D.R. Lloyd, S.S. Kim, K.E. Kinzer, Microporous membrane formation via thermally-induced phase separation. II. Liquid—liquid phase separation, J. Membr. Sci., 64 (1991) 1–11.
[3] S.S. Kim, D.R. Lloyd, Microporous membrane formation via thermally-induced phase separation. III. Effect of thermodynamic interactions on the structure of isotactic polypropylene membranes, J. Membr. Sci., 64 (1991) 13–29.
[4] T.H. Xiao, P. Wang, X. Yang, X. Cai, J. Lu, Fabrication and characterization of novel asymmetric polyvinylidene fluoride (PVDF) membranes by the nonsolvent thermally induced phase separation (NTIPS) method for membrane distillation applications, J. Membr. Sci., 489 (2015) 160–174.
[5] Q.Y. Wu, L.S. Wan, Z.K. Xu, Structure and performance of polyacrylonitrile membranes prepared via thermally induced phase separation, J. Membr. Sci., 409 (2012) 355–364.
[6] H.Q. Liang, Q.Y. Wu, L.S. Wan, X.J. Huang, Z.K. Xu, Polar polymer membranes via thermally induced phase separation using a universal crystallizable diluent, J. Membr. Sci., 446 (2013) 482–491.
[7] Z.L. Cui, N.T. Hassankiadeh, S.Y. Lee, Poly(vinylidene fluoride) membrane preparation with an environmental diluent via thermally induced phase separation, J. Membr. Sci., 444 (2013) 223–236.
[8] H. Matsuyama, M. Yuasa, Y. Kitamura, Structure control of anisotropic and asymmetric polypropylene membrane prepared by thermally induced phase separation, J. Membr. Sci., 179 (2000) 91–100.
[9] M.H. Gu, J. Zhang, X.L. Wang, H. Tao, L. Ge, Formation of poly(vinylidene fluoride) (PVDF) membranes via thermally induced phase separation, Desalination, 192 (2006) 160–167.
[10] L.S. Wu, J.F. Sun, Structure and properties of PVDF membrane with PES-C addition via thermally induced phase separation process, Appl. Surf. Sci., 322 (2014) 101–110.
[11] N. Han, J.C. Xiong, S.M. Chen, Structure and properties of poly (acrylonitrile-co-methyl acrylate) membranes prepared via thermally induced phase separation, J. Appl. Polym. Sci., 133 (2016) 1–8.

[12] H.Q. Liang, K.J. Ji, L.Y. Zha, Polymer membranes with vertically-oriented pores constructed by 2D freezing at ambient temperature, ACS Appl. Mater. Interfaces, 8 (2016) 14174–14181.
[13] N.N. Li, C.F. Xiao, S.M. Mei, S.J. Zhang, The multi-pore-structure of polymer–silicon hollow fiber membranes fabricated via thermally induced phase separation combining with stretching, Desalination, 274 (2011) 284–291.
[14] M.H. Shinde, S.S. Kulkarni, D.A. Musale, Improvement of the water purification capability of poly (acrylonitrile) ultrafiltration membranes, J. Membr. Sci., 162 (1999) 9–22.
[15] D.A. Musale, S.S. Kulkarni, Relative rates of protein transmission through poly (acrylonitrile) based ultrafiltration membranes, J. Membr. Sci., 136 (1997) 13–23.
[16] S. Azari, M. Karimi, M.H. Kish, Structural properties of the poly(acrylonitrile) membrane prepared with different cast thicknesses, Ind. Eng. Chemres., 49 (2010) 2442–2448.
[17] Z.G. Wang, L.S. Wan, Z.K. Xu, Surface engineerings of polyacrylonitrile-based asymmetric membranes towards biomedical applications: An overview, J. Membr. Sci., 304 (2007) 8–23.
[18] D. Pal, S. Neogi, S. De, Improved antifouling characteristics of acrylonitrile co-polymer membrane by low temperature pulsed ammonia plasma in the treatment of oil–water emulsion, Vacuum, 131 (2016) 293–304.
[19] F.Q. Nie, Z.K. Xu, L.S. Wan, Acrylonitrile-based copolymers containing reactive groups: synthesis and preparation of ultrafiltration membranes, J. Membr. Sci., 230 (2004) 1–11.
[20] P. Ye, Z.K. Xu, Z.G. Wang, Comparison of hydrolytic activities in aqueous and organic media for lipases immobilized on poly (acrylonitrile-co-maleic acid) ultrafiltration hollow fiber membrane, J. Mol. Catal. B: Enzym., 32 (2005) 115–121.
[21] C.H. Tsou, Q.F. An, S.C. Lo, Effect of microstructure of graphene oxide fabricated through different self-assembly techniques on 1-butanol dehydration, J. Membr. Sci., 477 (2015) 93–100.
[22] Y. Du, Y. Lv, W.Z. Qiu, Nanofiltration membranes with narrowed pore size distribution via pore wall modification, Chem. Commun., 52 (2016) 8589–8592.
[23] Q. Sun, Y. Su, X. Ma, Improved antifouling property of zwitterionic ultrafiltration membrane composed of acrylonitrile and sulfobetaine copolymer, J. Membr. Sci., 285 (2006) 299–305.
[24] Q.Y. Wu, B.T. Liu, M. Li, L.S. Wan, Z.K. Xu, Polyacrylonitrile membranes via thermally induced phase separation: Effects of polyethylene glycol with different molecular weights, J. Membr. Sci., 437 (2013) 227–236.
[25] N. Han, X.X. Zhang, Fabrication, structures, and properties of acrylonitrile/methyl acrylate copolymers and copolymers containing microencapsulated phase change materials, J. Appl. Polym. Sci., 103 (2007) 2776–2781.
[26] N. Han, X.X. Zhang, W.Y. Yu, Effects of copolymerization temperatures on structure and properties of melt-spinnable acrylonitrile-methyl acrylate copolymers and fibers, Macromol. Res., 18 (2010) 1060–1069.
[27] J.A. Ronner, S.G. Wassink, C.A. Smolders, Inversigation of liquid-liquid demixing and aggregate formation in a membrane forming system by means of pulse-induced critical scattering (PICS), J. Membr. Sci., 42 (1989) 27–36.
[28] J. Brandrup, E.H. Immergut, E.A. Grulke, Polymer Handbook, Wiley, New York, NY, 1999.
[29] R.G. Miller, C.Q. Bowles, C.C. Chappelow, Application of solubility parameter theory to dentin-bonding systems and adhesive strength correlations, J. Biomed. Mater. Res., 41 (1998) 237–243.
[30] M.J. He, W. Chen, X.X. Dong, Polymer physics, Fudan University Publishers, Shanghai, China, 1990.
[31] A. Bottino, G. Capannelli, S. Munari, Solubility parameters of poly (vinylidene fluoride), J. Polym. Sci. B: Polym. Phys., 26 (1988) 785–794.
[32] C.K. Kjellander, T.B. Nielsen, A. Ghanbari-Siahkali, ESC resistance of commercial grade polycarbonates during exposure to butter and related chemicals, Polym. Degrad. Stab., 93 (2008) 1486–1495.
[33] S. Yang, L. Zhongzhou, Preparation and characterization of polyacrylonitrile ultrafiltration membranes, J. Membr. Sci., 222 (2003) 87–98.
[34] A.I. Gopalan, P. Santhosh, K.M. Manesh, Development of electrospun PVdF-PAN membrane-based polymer electrolytes for lithium batteries, J. Membr. Sci., 325 (2008) 683–690.
[35] J. Feng, Z.L. Xu, H. Yang, Hydrophilic microporous PES membranes prepared by PES/PEG/DMAc casting solutions, J. Appl. Polym. Sci., 107 (2008) 4100–4108.
[36] S.W. Song, J.M. Torkelson, Coarsening effects on microstructure formation in isopycnic polymer solutions and membranes produced via thermally induced phase separation, Macromol., 27 (1994) 6389–6397.
[37] K.S. McGuire, A. Laxminarayan, D.R. Lloyd, Kinetics of droplet growth in liquid–liquid phase separation of polymer–diluent systems: experimental results, Polymer, 36 (1995) 4951–4960.
[38] H. Matsuyama, S. Berghmans, D.R. Lloyd, Formation of hydrophilic microporous membranes via thermally induced phase separation, J. Membr. Sci., 142 (1998) 213–224.
[39] G.L. Ji, L.P. Zhu, B.K. Zhu, Structure formation and characterization of PVDF hollow fiber membrane prepared via TIPS with diluent mixture, J. Membr. Sci., 319 (2008) 264–270.
[40] L. Wang, D. Huang, X. Wang, Preparation of PVDF membranes via the low-temperature TIPS method with diluent mixtures: The role of coagulation conditions and cooling rate, Desalination, 361 (2015) 25–37.
[41] C.Y. Liu, C.J. He, Preparation and characterization of polyacrylonitrile membranes with high strength via thermally induced phase separation process, Mater. Sci. Forum. Trans. Tech. Publications, 789 (2014) 205–208.
[42] N. Han, S.M. Chen, G. Chen, Preparation of poly (acrylonitrile-methacrylate) membrane via thermally induced phase separation: effects of MA with different feeding molar ratios, Desal. Water Treat., 57 (2016) 27531–27547.

Supporting Information

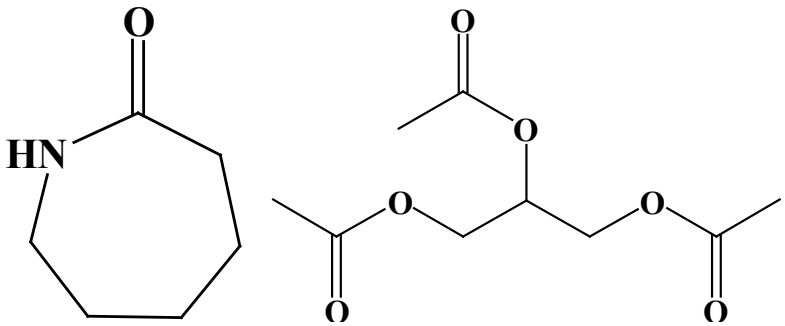

CPL GTA

Fig. S1. Chemical structures of CPL and GTA.

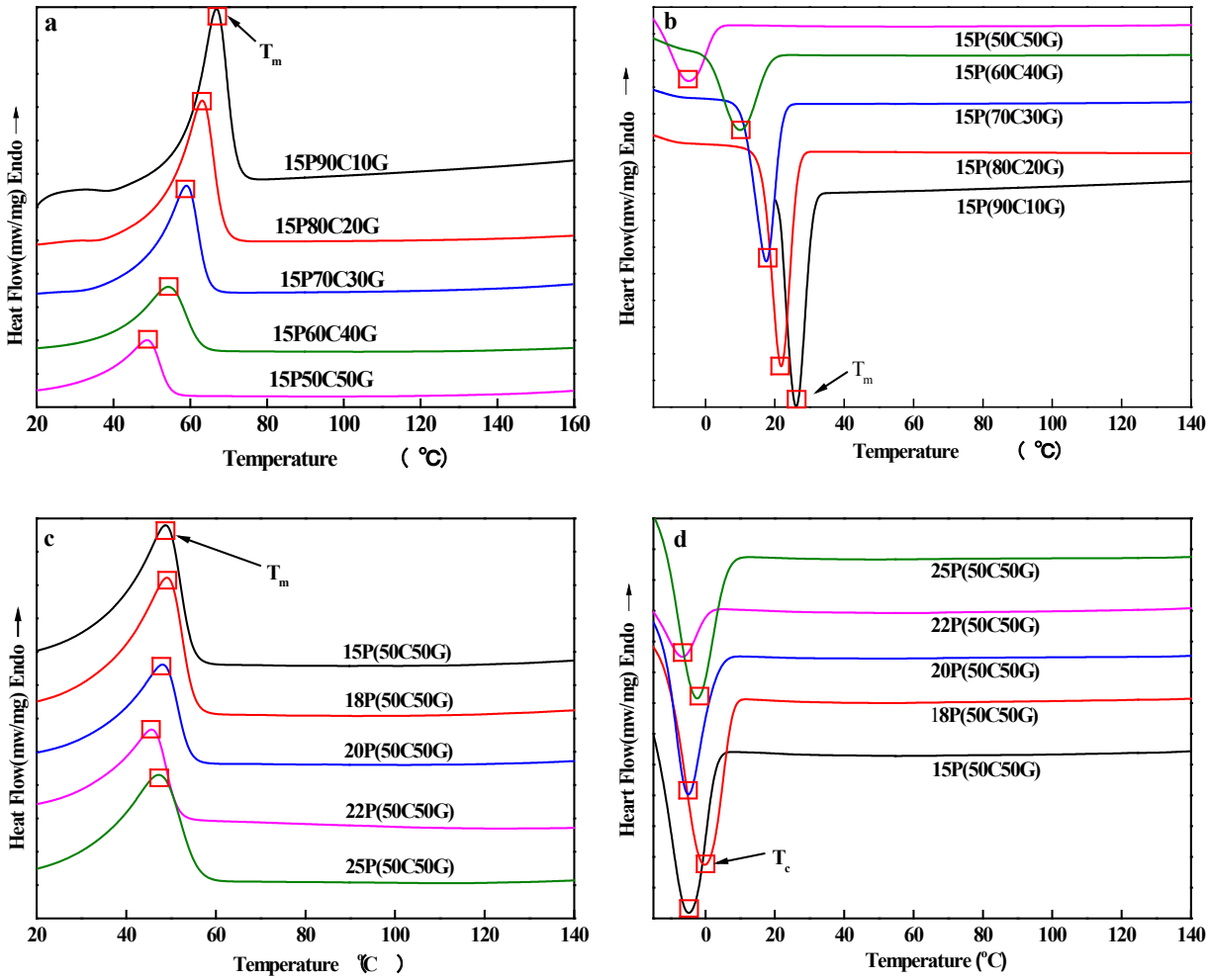

Fig. S2. Crystallization and melting behaviors of the P(AN-MA)/CPL/GTA ternary system with various P(AN-MA) and CPL content. (a), (c) DSC heating curves of P(AN-MA)/CPL/MPEG550 ternary system; (b), (d) DSC cooling curves of P(AN-MA)/CPL/MPEG550 ternary system.

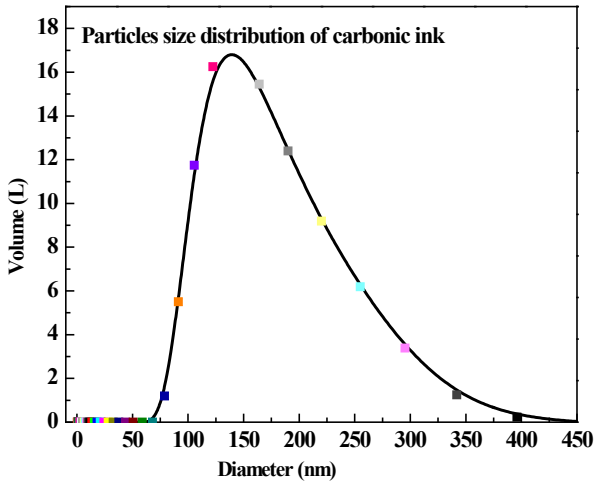

Fig. S3. The particle size distribution of the carbonic ink solution.

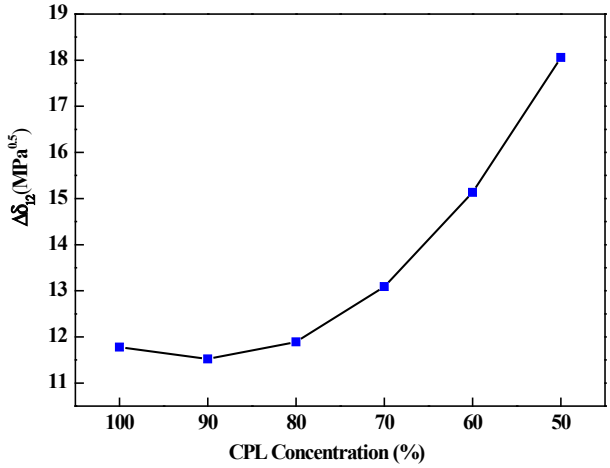

Fig. S4. The relationship cure between Δδ12 and CPL content in the mixed diluent.

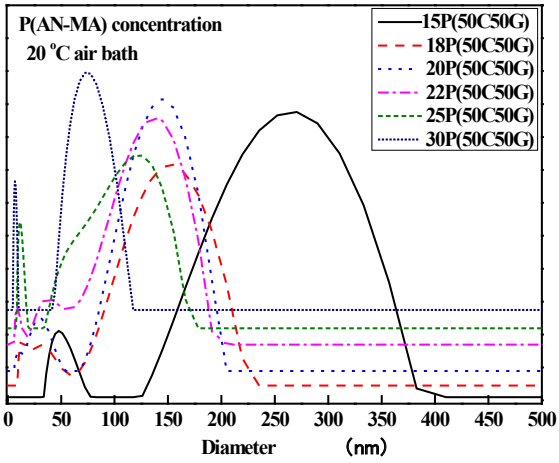

Fig. S5. The pore size distribution of P(AN-MA) membrane prepared with various polymer concentrations (20 °C air bath).

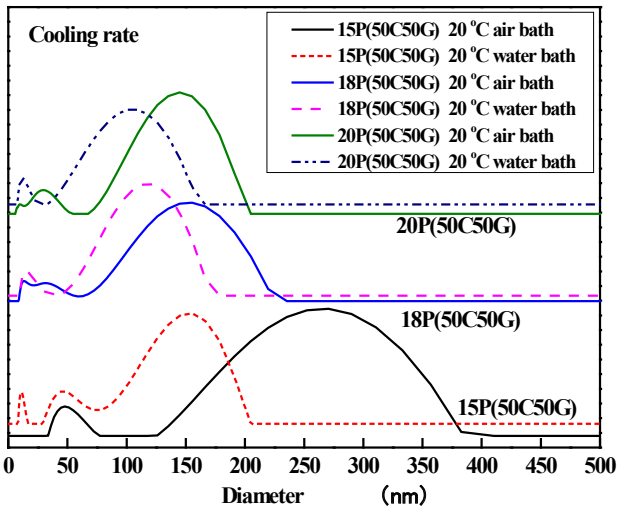

Fig. S6. The pore size distribution of P(AN-MA) membranes formed at different cooling rates. The solid lines represent membranes fabricated in an air bath, and the dash lines represent the membranes fabricated in a water bath.

Fig. S7. The feed solution and filtrate solution filtered by-20P(50C50G) membrane formed in20 °C air bath

Table S1
Crystallization temperature (T_c), melting point (T_m) of 15P(50C50C) mixture at different cooling rate

Cooling rate	Heating			Cooling		
	T_{mo} (°C)	T_{mp} (°C)	ΔH_m (J/g)	T_{co} (°C)	T_{cp} (°C)	ΔH_c (J/g)
10°C/min	35.9	48.8	38.0	2.9	–4.8	35.9
5°C/min	36.0	48.7	47.3	6.6	1.9	47.6
2°C/min	37.2	48.6	37.3	8.3	4.2	35.7

T_{mo} - The onset temperature of the melting peak; T_{mp} - The peak temperature of the melting peak; T_{co} - The onset temperature of the crystallization peak; T_{cp} - The peak temperature of the crystallization peak.

Table S2
Some typical properties of P(AN-MA) membranes prepared via TIPS

Sample	Coagulation bath	Porosity (%)	Water flux (L/m²·h)	Stress (MPa)	Average pore size(nm)	Rejection (%)
15P(50C50G)	20 °C, air	79.4	6802	2.80	270.5	91.9
18P(50C50G)	20 °C, air	69.7	5200	3.49	155.2	94.7
20P(50C50G)	20 °C, air	65.5	1604	4.74	144.8	95.3
15P(50C50G)	20 °C, water	75.5	1203	3.87	153.4	95.0
18P(50C50G)	20 °C, water	67.7	204	7.30	117.6	97.3
20P(50C50G)	20 °C, water	62.5	115	8.51	102.3	98.2